Energy & Environmental Science

PAPER

Cite this: *Energy Environ. Sci.*, 2014, **7**, 3808

Toward the rational benchmarking of homogeneous H_2-evolving catalysts

Vincent Artero*[a] and Jean-Michel Saveant*[b]

Received 2nd June 2014
Accepted 6th August 2014

DOI: 10.1039/c4ee01709a

www.rsc.org/ees

Molecular electrocatalysts for H_2 evolution are usually studied under various conditions (solvent and proton sources) that prevent direct comparison of their performances. We provide here a rational method for such a benchmark based on (i) the recent analysis of the current-potential response for two-electron-two-step mechanisms and (ii) the derivation of catalytic Tafel plots reflecting the interdependency of turnover frequency and overpotential based on the intrinsic properties of the catalyst, independent of contingent factors such as cell characteristics. Such a methodology is exemplified on a series of molecular catalysts among the most efficient in the recent literature.

Broader context

The future of energy supply depends on innovative breakthroughs regarding the design of cheap, sustainable and efficient systems for the conversion and storage of renewable energy sources, such as wind and solar energy. The production of hydrogen, a fuel with remarkable properties, through water splitting appears as a promising and appealing solution. Electro-catalysis is a key enabling technology in this context since the requirement for noble metal-based catalysts (Pt, IrO_2…) is the main limitation for electrolysis and fuel-cell technologies to become economically viable. A number of earth-abundant molecular catalysts for hydrogen evolution, some of them inspired by the structure of the active site of hydrogenase enzymes, have been reported during the last two decades and we provide here a methodology to assess their catalytic performances, which appears as a prerequisite before immobilization of these catalysts into electrode materials, that may be further implemented in technological devices such as electrolyzers or photo-electrocatalytic cells.

Introduction

Transition towards a post-oil economy depends on our capacity to find new sustainable solutions for exploiting renewable energies such as sun or wind.[1] In this context, the production of fuels is appealing since their stability and mass energetic content are orders of magnitude higher than those of batteries or supercapacitors.[2,3] Hydrogen (H_2) has been set as the first target for such solar- or electro-fuels in the perspective of the dawn of the hydrogen economy.[4]

Hydrogen production from water is a multi-step two-electron process which requires catalysis to occur both at fast rates and near thermodynamic equilibrium, these two conditions being mandatory for efficient power to chemical energy transduction. While platinum and other noble metals already meet the above mentioned specifications as H_2-evolving electrocatalysts, the development of earth-abundant electrocatalysts[5–7] is a requisite for this approach to become economically viable. Many molecular compounds based on Ni,[8,9] Fe,[6,10,11] Co (ref. 12) or Mo[13–15] complexes, often inspired by the structure or function of the active sites of hydrogenases,[16,17] have been reported in the past 15 years as active catalysts for H_2 evolution. However, the conditions used for assessing activity are almost as varied as the catalysts themselves and it is urgent to establish a rational way to benchmark homogeneous H_2-evolving catalysts. Several previous attempts in that direction focused on the notion of "onset" or "operating" potential, which has the interest of providing a quick estimate of the maximal (in reduction reactions) or minimal (in oxidation reactions) electrode potential at which catalysis takes place. Several definitions of the onset/operating potential have been proposed.[18–24] However, comparison between catalysts does not only require the definition of the potential at which catalysis takes place but also some measure of the catalytic rate at this electrode potential. In this respect, it seems natural to rely on a classical notion of homogeneous catalysis, namely the turnover frequency (TOF). This has however to be adapted to the homogeneous catalysis electrochemical context in two ways. One is to take into account the fact that the catalyst molecules that effectively partake in catalysis are not all the molecules present in the cell compartment but only those contained in a thin reaction-diffusion layer adjacent to the electrode, whose thickness is a decreasing function of the catalysis rate. The catalysis rate thus governs the TOF both in determining the rate at which the substrate is transformed and also the number of catalyst molecules actually

[a]*Univ Grenoble Alpes, CNRS and CEA, Laboratoire de Chimie et Biologie des Métaux, 17 rue des martyrs, 38000 Grenoble, France. E-mail: vincent.artero@cea.fr*

[b]*Université Paris Diderot, Sorbonne Paris Cité, Laboratoire d'Electrochimie Moléculaire, Unité Mixte de Recherche Université – CNRS No 7591, Bâtiment Lavoisier, 15 rue Jean de Baïf, 75205 Paris Cedex 13, France. E-mail: saveant@univ-paris-diderot.fr*

involved, a specific feature of electro-assisted catalysis.[25] The second adaptation derives from the dependence of the TOF thus defined on the electrode potential, and therefore from the overpotential, classically defined as the absolute value of the difference between the electrode potential and the apparent standard potential of the reaction to be catalyzed.[25,26] The "catalytic Tafel" plots relating the TOF to the overpotential thus provide a means of comparing the catalysts though their intrinsic properties, independent of the characteristics of the electrochemical cell. Without neglecting another important factor of merit of a catalyst, *viz.*, its stability, we focus in the following on benchmarking the catalyst by comparison of its catalytic Tafel plots.[25–27] We first provide reminders on the foundations needed to establish such "catalytic Tafel plots" for homogeneous electrocatalysts and then illustrate the application of this approach by examples of previously reported H_2-evolving catalysts for which consistent, reliable and relevant data can be found in the literature.

Results and discussion

1. Turnover frequency and overpotential

The turnover number is defined as the number of catalytic cycles achieved by a single catalyst. The total turnover number (tTON) is defined as the TON achieved before full degradation of the catalyst.

The turnover frequency (TOF) is the number of turnovers achieved in a unit of time, during the period of time where degradation of the catalyst remains negligible. The TOF may then be obtained from the ratio of the number of moles of product, generated per unit of time to the number of moles of the catalyst.

The determination of TON and TOF always requires the knowledge of the number of catalytic active sites, which is often an issue in the case of heterogeneous catalysis. This problem does not exist in homogeneous catalysis but, in this case, it is necessary to know the amount of catalyst active in the immediate vicinity of the electrode that effectively participates in catalysis as discussed in more detail later on.

The overpotential (η) is a thermodynamic quantity simply equal to the difference between the electrode potential E and the apparent standard potential of the reaction to be catalyzed. In the case of reduction of protons, the overpotential is written as follows:

$$\eta = E^{0,\mathrm{ap}}_{\mathrm{H^+/H_2}} - E$$

The determination of $E^{0,\mathrm{ap}}_{\mathrm{H^+/H_2}}$ has been the subject of several reports.[20,22,28] This value is generally computed from two tabulated values, $E^{0}_{\mathrm{H^+/H_2}}$, the standard potential of the H^+/H_2 couple in the solvent used for the study and the pK_a of the proton source in the same solvent:

$$E^{0,\mathrm{ap}}_{\mathrm{H^+/H_2}} = E^{0}_{\mathrm{H^+/H_2}} - 0.059\mathrm{p}K_a$$

The pK_a values for a number of acids are known,[29] albeit in a restricted number of solvents. The same is true for the standard potential of the H^+/H_2 couple, which is only known in CH_3CN, DMF and DMSO (Table 1 of ref. 22). Of note, an initially reported value[30] has been corrected to account for the stoichiometry of the reaction[22] and the new value was confirmed by measurements carried out on bidirectional homogeneous electrocatalysts for H^+/H_2 interconversion.[31] More recently an electrochemical method was reported that allows the direct determination of $E^{0,\mathrm{ap}}_{\mathrm{H^+/H_2}}$, provided that the H^+/H_2 equilibrium can be reached at the working electrode plunged in the solvent of the study in the presence of the proton source and H_2 gas.[32] Within the 50 mV error range of this method, the $E^{0,\mathrm{ap}}_{\mathrm{H^+/H_2}}$ values thus obtained are similar to those obtained from tabulated values in CH_3CN and DMF.[22] This method, which requires the use of a special Pt electrode annealed under H_2, is nevertheless valuable to get values of $E^{0,\mathrm{ap}}_{\mathrm{H^+/H_2}}$ for specific solvent–proton source combinations for which no tabulated values are available.

Acids (AH) and their conjugate base (A^-) often form stable adducts (AHA^-) through hydrogen bonding.[33,34] This phenomenon, called homoconjugation,[35] depends on the concentration of the acid. It is very frequent in acetonitrile and present to a lesser extent in DMF.[29] The influence of homoconjugation on $E^{0,\mathrm{ap}}_{\mathrm{H^+/H_2}}$ has been described in detail and is used in this study (see ref. 22 and footnote h of Table 1).

2. Catalytic Tafel plots

Molecular homogeneous catalysis of H_2 evolution is a multi-electron multi-step process. It is nevertheless useful to recall basic notions that are easier to introduce with the help of a simplified one-electron-one step reaction scheme such as the one depicted in Scheme 1.[36,37]

If the catalytic reaction is fast and irreversible, a steady-state situation is established by mutual compensation between catalytic reaction and diffusional transport. It results in "pure kinetic conditions" implying that the concentration profiles of both forms of the catalyst are confined within a thin reaction-diffusion layer, whose thickness is of the order of $\sqrt{D_{\mathrm{cat}}/k_{\mathrm{cat}}}$ (D_{cat} is the diffusion coefficient of the catalyst). This entails that, in the definition of the catalyst turnover number (TON) and turnover frequency (TOF), the number of moles of catalyst that are actually involved are those contained in the reaction layer rather than in the whole solution.[38] If the substrate is in such excess that its consumption may be neglected and if the electrode electron transfer that generates the active form of the catalyst is so fast that the Nernst law is obeyed, an S-shaped current potential response will be observed:

$$i = \frac{i_{\mathrm{pl}}}{1 + \exp\left[\dfrac{F}{RT}\left(E - E_{1/2}\right)\right]} \quad (1)$$

with a half-wave potential

$$E_{1/2} = E^{0}_{\mathrm{cat}} \quad (2)$$

and with a plateau current, independent of the scan rate:

$$i_{pl} = FSC^0_{cat}\sqrt{D_{cat}}\sqrt{k_{cat}C^0_{subst}} \quad (3)$$

where S is the electrode surface area and C^0_S is the bulk concentrations of the subscript species.[36,37] These equations apply not only to non-destructive electrochemical techniques, such as cyclic voltammetry, but also, if the catalyst is stable enough, under preparative-scale conditions regardless of the cell-time response.[39]

During the period of time where the catalyst remains stable, the turnover frequency, TOF, may then be obtained from the ratio:

$$\mathrm{TOF} = \frac{N_{\mathrm{product}}}{N_{\mathrm{active\ cat}}}$$

of the number of moles of product, generated per unit of time to the maximal number of moles of the active forms of the catalyst contained in the reaction-diffusion layer. TOF has thus the dimension of $(\mathrm{time})^{-1}$.

It follows that:[25–27]

$$\mathrm{TOF} = \frac{\mathrm{TOF}_{max}}{1+\exp\left[\frac{F}{RT}\left(E-E_{1/2}\right)\right]} \quad (4)$$

with:

$$\mathrm{TOF}_{max} = k_{cat}C^0_{subst} \quad (5)$$

Introducing the overpotential η (as already defined above), the catalytic Tafel plot is thus obtained as:

$$\mathrm{TOF} = \frac{\mathrm{TOF}_{max}}{1+\exp\left[\frac{F}{RT}\left(E^0_{H^+/H_2}-E_{1/2}\right)\right]\exp\left(-\frac{F}{RT}\eta\right)} \quad (6)$$

To be plotted in the logarithmic form as shown schematically in Fig. 1. The resulting characteristic curve is most conveniently derived from non-destructive experiments such as CV recordings. It is however important to check that preparative-scale experiments, in which the potential or the current is imposed and the resulting current or potential is measured, lead to concordant results. Such preparative-scale data are pictured as stars in Fig. 1.

What changes when the catalytic process involves several electron transfers and several chemical steps, *e.g.*, two electron transfers and two chemical steps as is the case with hydrogen evolution catalysts? The various types of reaction mechanisms can be categorized according to the succession of electron transfer steps, E, and chemical steps, C (at least one of which involves a proton transfer in the present case). In this context, a C step is not necessarily a single elementary step. It may well consist of an association of elementary steps, reversible or not, the whole reaction being globally irreversible and characterized by an apparent rate constant. A couple of illustrating examples of this categorization is shown in Scheme 2.

In both cases, eqn (1), (4) and (6) still hold, whereas eqn (2), (3) and (5) are replaced by:[27]

$$\mathrm{EECC}: E_{1/2} = E^0_2 + \frac{RT}{F}\ln\left(1+\sqrt{\frac{k_1}{k_2}}\frac{1}{1+\sqrt{\frac{k_1}{k_2}}}\right) \quad (7)$$

$$\mathrm{ECEC}: E_{1/2} = E^0_1 + \frac{RT}{F}\ln\left(1+\sqrt{\frac{k_1}{k_2}}\right) \quad (7')$$

$$\mathrm{EECC}: i_{pl} = 2FSC^0_{cat}\sqrt{D_{cat}}\frac{\sqrt{k_1[\mathrm{AH}]}}{1+\sqrt{\frac{k_1}{k_2}}\frac{1}{1+\sqrt{\frac{k_2}{k_1}}}} \quad (8)$$

or:

$$\frac{i_{pl}}{i^0_p} = 4.48\frac{\sqrt{k_1[\mathrm{AH}]}}{1+\sqrt{\frac{k_1}{k_2}}\frac{1}{1+\sqrt{\frac{k_2}{k_1}}}}\sqrt{\frac{RT}{Fv}}$$

where i^0_p is the peak current of a one-electron reversible

$$\mathrm{Nernstian\ wave}: i^0_p = 0.446FSC^0_{cat}\sqrt{D_{cat}}\sqrt{\frac{Fv}{RT}}$$

$$\mathrm{ECEC}: i_{pl} = 2FSC^0_{cat}\sqrt{D_{cat}}\frac{\sqrt{k_1k_2[\mathrm{AH}]}}{\sqrt{k_1}+\sqrt{k_2}} \quad (8')$$

or:

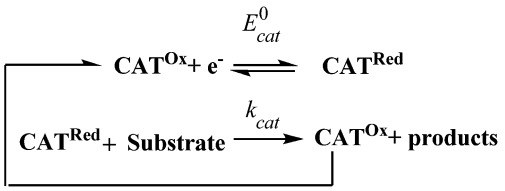

Scheme 1 Simplified catalytic scheme.

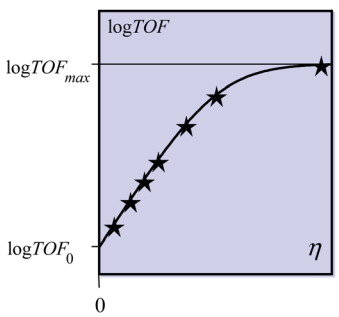

Fig. 1 An example of the catalytic Tafel plot for the simplified reaction scheme (Scheme 1). The solid line is a graphical representation of eqn (6) as can be derived from the values of TOF_{max} and $E_{1/2}$ resulting, *e.g.*, from cyclic voltammetry measurements. The stars pictured the data that can be obtained from a series of preparative-scale experiments as a check of the predictions based on cyclic voltammetric data. These electrolyses also allow one to test the stability of the catalyst.

$$\frac{i_{pl}}{i_p^0} = 4.48\frac{\sqrt{k_1 k_2[AH]}}{\sqrt{k_1}+\sqrt{k_2}}\sqrt{\frac{RT}{Fv}} \quad (8')$$

Then, in both cases,

$$TOF_{max} = \frac{k_1 k_2}{k_1 + k_2}[AH] \quad (9)$$

The other cases are analyzed in ref. 27 and procedures to set up the catalytic Tafel plots are proposed, based on the determination of the two standard potentials and the two apparent rate constants. As in the simplified case, points located in the top left zone of the log TOF – η plane represent the best catalysts and *vice versa* for the bottom right zone.

We examine in the next section the behavior of several examples of H_2-evolving catalysts described in the current literature. They were selected among more numerous cases on the basis that enough data were available to determine the characteristic rate constants and potentials and, from there, the log TOF – η plots featuring each of them. In this endeavor, difficulties, related to "side-phenomena," are often encountered, which make the CV responses peak-shaped and scan rate dependent when a scan-rate independent S-shaped response is expected. As discussed in detail elsewhere, these side phenomena may have various origins – consumption of the substrate (here the acid AH), inhibition by products,[40,25] deactivation of the catalyst and, more generally, phenomena that parallel the efficiency of catalysis.[25]Among them, the easiest to treat is the case where the consumption of the catalyst occurs and occurs alone. The zone diagram in Fig. 2 recalls the way in which substrate consumption may influence the CV responses, still taking as an example the simplified reaction scheme (Scheme 1). On the top of the diagram, where the pure kinetic conditions are achieved as they are for fast catalytic processes, the system passes, upon increasing the catalytic rate constant and decreasing the excess of substrate over catalyst, from the canonical S-shape to the "total" catalysis situation. In all cases then, the characteristics of the CV responses are known and can be used to derive the relevant rate constant and therefrom, the turnover frequency. We will see in Section 2 how these procedures can be extended to two-electron-two-step processes in each case that will be treated.

Other side-phenomena, which may occur at the same time or instead of substrate consumption, are much more difficult to identify and treat. One way out of these difficulties is to focus on the foot of the CV wave where the contributions of all side-phenomena are minimal.[25,26,42] Another way is to raise the scan rate so as to decrease the charge passed during the experiment and thus minimize all the side-phenomena. These two strategies may also be applied simultaneously.

In the above discussion, we have only considered heterolytic mechanisms, *i.e.*, mechanisms in which dihydrogen results from the reaction of a metal-hydride on the acid, rather than from the reaction of two molecules of the metal-hydride during which two hydrogen atoms combine to give hydrogen, as it occurs in homolytic mechanisms. The reason for this simplification is that, as shown recently,[43] heterolytic pathways predominate over homolytic pathways for strong or moderately strong acids as in the examples we discuss in the next section.

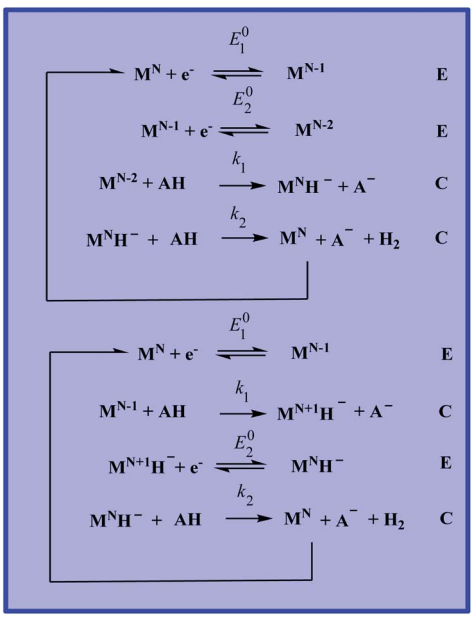

Scheme 2 Two examples of two-electron-two-step catalytic reaction schemes (a): M^J: metal complex at the oxidation degree J, AH: proton donor, and A^-: conjugate base. E_1^0 and E_2^0: standard potentials. k_1 and k_2: second order rate constants.

3. Examples of benchmarking of some homogeneous H_2-evolving catalysts

Establishing a catalytic Tafel plot for a given catalyst derives from the application of eqn (6), which implies knowing $E_{1/2}$ and TOF_{max}. All potentials involved are preferably referred to the Fc^+/Fc couple in the solvent as is the value of E^0_{H/H_2}. TOF_{max} and all TOF values are reported in s^{-1} as second order kinetic constants taken for 1 M of acid. Estimation of these two parameters requires the value of the rate constants k_1 and k_2 (eqn (9)).

The methodology presented here is general and can be applied to benchmark any H_2-evolution catalyst provided (i) it has been characterized in a solvent from which overpotential values can be reliably determined and (ii) kinetic data pertaining to a relevant mechanistic scheme are available. In the course of this study, we examined the vast literature on molecular H_2-evolving catalysts and, in many cases, could not find all data required for the construction of catalytic Tafel plots. In most cases indeed, kinetic data are extracted using eqn (3) while the system is not in the "pure kinetic" regime which precludes utilization of such data for benchmarking purposes. We finally selected only a few systems, listed in Table 1 for which we could extract reliable data for the construction of catalytic Tafel plots. Data in Table 1 and the ensuing catalytic Tafel plots in Fig. 4 therefore do not intend to cover all reported homogeneous H_2-evolving catalysts but simply to serve as examples of benchmarking procedures based on the intrinsic properties of

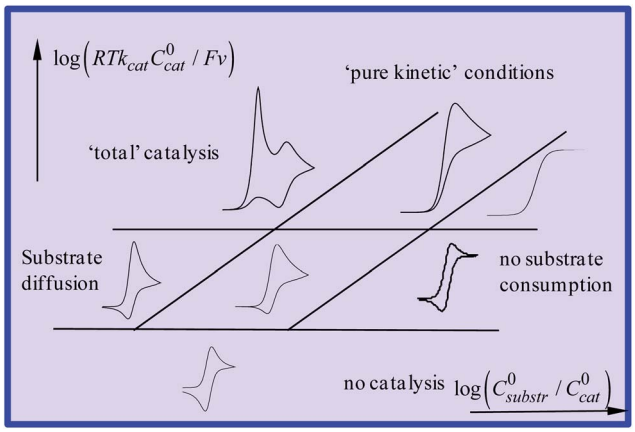

Fig. 2 Catalytic zone diagram for the simplified reaction scheme (Scheme 1).[37,41]

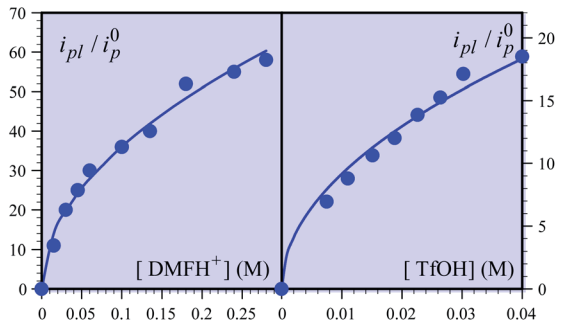

Fig. 3 Catalysis of H_2 evolution from the reduction of $DMFH^+$ and TfOH in acetonitrile by $Ni^{II}[(P_2^{Ph}N_2^{C_6H_4X})_2]$. Variation of the normalized plateau with the concentration of acid. Left: X = $CH_2P(O)(OEt)_2$. Dots: experimental data (from Fig. 3 in ref. 46; data measured at 50 mV s^{-1}). Solid line: proportionality to $\sqrt{[DMFH^+]}$ with a proportionality factor of 114 $M^{-1/2}$ right: X = H. Dots: experimental data (from Fig. 3 in ref. 21; data measured at 50 mV s^{-1}). Solid line: proportionality to $\sqrt{[TfOH]}$ with a proportionality factor of 92.

the catalysts freed of the particular specifications of the electrolysis cell that was used.

In the case of $Fe^{II}TPP$,[44] the reaction pathway was shown to be of the EECC type. Besides the values of the standard potentials, one can thus use the reported values of k_1 and k_2, which were derived from analysis of the CV responses at low acid concentrations, where the "total catalysis" conditions (see the top left zone in Fig. 2) are fulfilled. These values are gathered in Table 1. TOF_{max} was then obtained by the application of eqn (6) with [AH] = 1 M and $E_{1/2}$ from eqn (7).

The $Co^{II}(dmgH)_2py$ complex ($dmgH_2$ = dimethylglyoxime and py: pyridine)[18] is another interesting case. It was originally analyzed in the framework of an ECCE mechanism, under conditions close to pure kinetic behavior. Re-examination of the data showed however that an ECEC mechanism also leads to a satisfactory fit of the CV data in agreement with the prediction[45–47] that the standard potential for the reduction of the first protonated intermediate (E_2^0 in lower Scheme 2) is more positive than the standard potential of the initial electron transfer step (E_1^0 in lower Scheme 2). The values of the various parameters thus obtained are listed in Table 1, leading to the corresponding Tafel plot in Fig. 3.

A different approach was used for the other catalysts of the list. It was based on CV responses pertaining to the S-shaped canonical behavior (top right corner of the zone diagram in Fig. 2). The first example in this category is $[Ni(P_2^{Ph}N^{Ph})_2]^{2+}$ represented in Chart 1.[48] S-shaped waves, independent of the scan rate, are observed for this catalyst in the presence of $DMFH^+$ in acetonitrile at the level of the Ni^{II}/Ni^{I} wave. Examination of the data in Fig. 4 of ref. 48 shows that $E_{1/2}$ is very close to the standard potential of the Ni^{II}/Ni^{I} couple. The most likely mechanism, in line with previous analysis,[9] thus belongs to the ECEC category (Scheme 2), with the second proton transfer being faster than the first, and the second electron transfer

Table 1 Examples of data treatment for some examples of literature H_2-evolving catalysts

Catalyst[g]	Acid	Solvent	$E^0_{H^+/H_2}$ [a,b]	Standard potentials[a] E_1^0, E_2^0	Rate constants[c] k_1, k_2	$E_{1/2}$ [a,f]	TOF_{max} ($[H^+]$ = 1 M)	Reaction scheme for TOF estimation	Ref.
$Fe^{II}TPP$[g]	Et_3NH^+	DMF	−1.20	−1.45, −2.16	2×10^8, 4×10^5[d]	−2.08	4×10^5	EECC	44
$Co^{II}(dmgH)_2py$[g]	Et_3NH^+	DMF	−1.20	−1.53, $E_2^0 > E_1^0$	10^4, $k_2 \gg k_1$[d]	−1.53	10^4	ECEC	18
$[Ni^{II}(P_2^{Ph}N^{Ph})_2]^{2+}$	$DMFH^+$	MeCN	−0.50[h]	−1.16, $E_2^0 > E_1^0$	7.5×10^4, $k_2 \gg k_1$[e]	−1.16	7.5×10^4	ECEC	48
$[Ni^{II}(P_2^{Ph}N_2^{C_6H_4X})_2]^{2+}$	$DMFH^+$	MeCN	−0.50[h]	−0.84, $E_2^0 > E_1^0$	1.3×10^3, $k_2 \gg k_1$[e]	0.84	1.3×10^3	ECEC	49
X= $CH_2P(O)(OEt)_2$									
H	TfOH	MeCN	−0.26	−0.85, $E_2^0 > E_1^0$	8×10^2, $k_2 \gg k_1$[e]	−0.85	8×10^2	ECEC	21

[a] In V *vs.* Fc^+/Fc. [b] Calculated for 1 M proton concentration from ref. 23, taking the homoconjugation effect into consideration, see text. [c] In eqn (7)–(9), $k_1^{ap} = k_1[AH]$ and $k_2^{ap} = k_2[AH]$, unless otherwise stated. k_1, k_2 in M^{-1} s^{-1}. [d] From the analysis of CV responses taking into account acid consumption under conditions of "total catalysis" or close to these conditions (see Fig. 2). [e] From the estimated plateau current, when the CV responses are S-shaped or close to be S-shaped. [f] $E_{1/2}$ may have two different meanings. It is either the observed half-wave potential of the CV response in the case depicted by footnote (e). It is then used, together with the plateau current to derive by means of eqn (7) and (8), the two rate constants. It may conversely be a calculated value when the two rate constants have been accessed in a different manner as in footnote (e), serving to establish the TOF – η relationship according to eqn (6), (7) and (9). [g] H_2TPP: tetraphenylporphyrin; $dmgH_2$: dimethylglyoxime; py: pyridine; $Co^{II}(dmgH)_2py$ is obtained from $Co^{III}(dmgH)_2pyCl$ after reductive elimination of Cl^-.[18] [h] The presence of an equimolar amount of the conjugate base DMF has been taken into consideration for the calculation of $E^0_{H^+/H_2}$ in a similar way to that described in ref. 22: in this specific case, the value of ε_D should be set at 17 ± 5 mV.

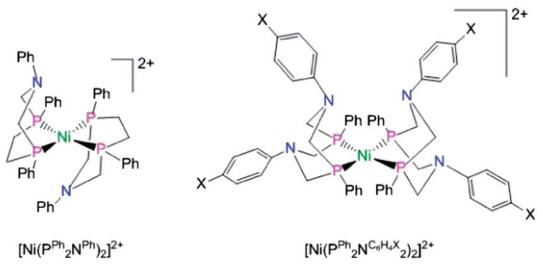

Chart 1

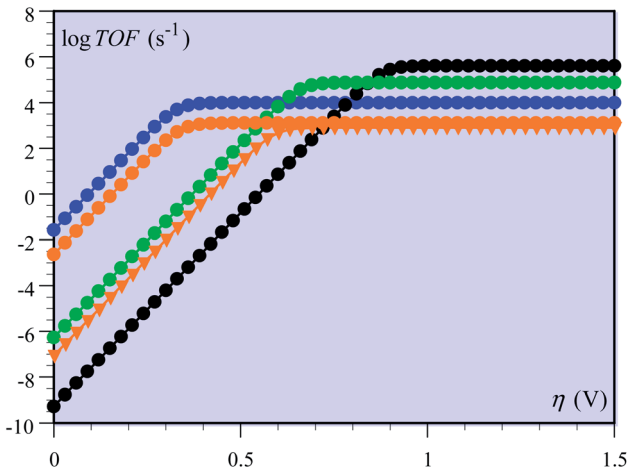

Fig. 4 Catalytic Tafel plots for the various electrocatalysts listed in Table 1. Black: Fe^{II}TPP, DMF, and Et_3NH^+. Blue: $Co^{II}(dmgH)_2py$, DMF, and Et_3NH^+. Green: $[Ni(P_2^{Ph}N^{Ph})_2]^{2+}$, MeCN, and $DMFH^+$. Orange: $[Ni^{II}(P_2^{Ph}N_2^{C_6H_4X})_2]^{2+}$ and MeCN, X = $CH_2P(O)(OEt)_2$, $DMFH^+$ (dots), X = H and TfOH (triangles).

easier than the first. This is confirmed by the proportionality of the apparent rate constant k_1^{ap} to the acid concentration (Fig. S8 of ref. 48). From the reported value of $i_{pl}/i_p^0 = 38$ for [AH] = 0.43 M and 10 V s^{-1}, $k_1 = 7.5 \times 10^4$ M^{-1} s^{-1} is derived from eqn (8″), considering that $k_2 \gg k_1$. TOF_{max} is then obtained from eqn (9) for [AH] = 1 M, which leads to the catalytic Tafel plot in Fig. 4.

A similar behavior is observed with another catalyst in a similar albeit different series, $[Ni^{II}(P_2^{Ph}N_2^{C_6H_4X})_2]^{2+}$ (Chart 1), in which X = $CH_2P(O)(OEt)_2$.[49] Here too, k_1 is proportional to the acid concentration as resulting from the variation of the normalized plateau current with the acid concentration, showing no saturation kinetics (Fig. 3, left). From the proportionality factor between i_{pl}/i_p^0 and $\sqrt{[DMFH^+]}$, the values of k_1 can be derived from eqn (8″) considering again that $k_2 \gg k_1$. TOF_{max} reported in Table 1 ensues as well as the resulting Tafel plot in Fig. 4.

Another example in the same series with X = H, but with a different acid (TfOH), is also very similar (Fig. 3, right), leading to the values in Table 1 and the Tafel plot in Fig. 4.[21]

Conclusions

Good electrocatalysts are defined by fast turn-over at low overpotential. In other words, catalysts displaying high turnover frequencies at the expense of large overpotentials will not allow for a good power-to-chemical conversion yield while those exhibiting low catalytic rates, even near the thermodynamic equilibrium, will not allow for the development of powerful electrocatalytic devices for the production of solar- or electrofuels. Catalytic Tafel plots provide a unified way to assess that these two properties are observed simultaneously with traces associated with the best catalysts appearing in the top-left corner of these graphs.

This rational way of benchmarking homogeneous H_2-evolving catalysts in the form of catalytic Tafel plots that relate the properly defined turnover frequency to the overpotential renders the comparison between catalysts independent of the characteristics of the particular electrochemical cell used and allows comparison of catalysts assayed under distinct experimental conditions (solvent and proton source), *viz.* without defining standard conditions of measurement.[50] Such plots can be acquired conveniently by non-destructive methods such as CV and then be used to optimize the preparative scale conditions, trading the balance between speed and energy consumption. This approach should be supplemented by testing comparatively the stability of the catalyst.

Acknowledgements

This work was supported by the French National Research Agency (Labex program, ARCANE, ANR-11-LABX-0003-01), the FCH Joint Undertaking (ArtipHyction Project, grant agreement no. 303435) and the European Research Council under the European Union's Seventh Framework Programme (FP/2007–2013)/ERC grant agreement no. 306398. The authors thank Vincent Fourmond (BIP, Marseille) for additional computation related to ref. 23.

Notes and references

1 A. Thapper, S. Styring, G. Saracco, A. W. Rutherford, B. Robert, A. Magnuson, W. Lubitz, A. Llobet, P. Kurz, A. Holzwarth, S. Fiechter, H. de Groot, S. Campagna, A. Braun, H. Bercegol and V. Artero, *Green*, 2013, **3**, 43.
2 T. A. Faunce, W. Lubitz, A. W. Rutherford, D. MacFarlane, G. F. Moore, P. Yang, D. G. Nocera, T. A. Moore, D. H. Gregory, S. Fukuzumi, K. B. Yoon, F. A. Armstrong, M. R. Wasielewski and S. Styring, *Energy Environ. Sci.*, 2013, **6**, 695–698.
3 T. Faunce, S. Styring, M. R. Wasielewski, G. W. Brudvig, A. W. Rutherford, J. Messinger, A. F. Lee, C. L. Hill, H. de Groot, M. Fontecave, D. R. MacFarlane, B. Hankamer, D. G. Nocera, D. M. Tiede, H. Dau, W. Hillier, L. Wang and R. Amal, *Energy Environ. Sci.*, 2013, **6**, 1074–1076.
4 N. Armaroli and V. Balzani, *ChemSusChem*, 2011, **4**, 21–36.
5 P. W. Du and R. Eisenberg, *Energy Environ. Sci.*, 2012, **5**, 6012–6021.
6 J. R. McKone, S. C. Marinescu, B. S. Brunschwig, J. R. Winkler and H. B. Gray, *Chem. Sci.*, 2014, **5**, 865–878.
7 V. S. Thoi, Y. J. Sun, J. R. Long and C. J. Chang, *Chem. Soc. Rev.*, 2013, **42**, 2388–2400.

8 S. Canaguier, V. Artero and M. Fontecave, *Dalton Trans.*, 2008, 315–325.
9 D. L. DuBois, *Inorg. Chem.*, 2014, **53**, 3935–3960.
10 J. F. Capon, F. Gloaguen, F. Y. Petillon, P. Schollhammer and J. Talarmin, *Coord. Chem. Rev.*, 2009, **253**, 1476–1494.
11 M. Beyler, S. Ezzaher, M. Karnahl, M. P. Santoni, R. Lomoth and S. Ott, *Chem. Commun.*, 2011, **47**, 11662–11664.
12 V. Artero, M. Chavarot-Kerlidou and M. Fontecave, *Angew. Chem., Int. Ed.*, 2011, **50**, 7238–7266.
13 H. I. Karunadasa, C. J. Chang and J. R. Long, *Nature*, 2010, **464**, 1329–1333.
14 H. I. Karunadasa, E. Montalvo, Y. J. Sun, M. Majda, J. R. Long and C. J. Chang, *Science*, 2012, **335**, 698–702.
15 A. Hijazi, J. C. Kemmegne-Mbouguen, S. Floquet, J. Marrot, J. Fize, V. Artero, O. David, E. Magnier, B. Pegot and E. Cadot, *Dalton Trans.*, 2013, **42**, 4848–4858.
16 T. R. Simmons and V. Artero, *Angew. Chem., Int. Ed.*, 2013, **52**, 6143–6145.
17 T. R. Simmons, G. Berggren, M. Bacchi, M. Fontecave and V. Artero, *Coord. Chem. Rev.*, 2014, **270–271**, 127–150.
18 M. Razavet, V. Artero and M. Fontecave, *Inorg. Chem.*, 2005, **44**, 4786–4795.
19 X. Hu, B. M. Cossairt, B. S. Brunschwig, N. S. Lewis and J. C. Peters, *Chem. Commun.*, 2005, 4723–4725.
20 G. A. N. Felton, R. S. Glass, D. L. Lichtenberger and D. H. Evans, *Inorg. Chem.*, 2006, **45**, 9181–9184.
21 A. D. Wilson, R. H. Newell, M. J. McNevin, J. T. Muckerman, M. Rakowski DuBois and D. L. DuBois, *J. Am. Chem. Soc.*, 2006, **128**, 358–366; X. Hu, B. S. Brunschwig and J. C. Peters, *J. Am. Chem. Soc.*, 2007, **129**, 8988–8998.
22 A. D. Wilson, R. H. Newell, M. J. McNevin, J. T. Muckerman, M. Rakowski DuBois and D. L. DuBois, *J. Am. Chem. Soc.*, 2006, **128**, 358–366.
23 V. Fourmond, P.-A. Jacques, M. Fontecave and V. Artero, *Inorg. Chem.*, 2010, **49**, 10338–10347.
24 C. N. Valdez, J. L. Dempsey, B. S. Brunschwig, J. R. Winkler and H. B. Gray, *Proc. Natl. Acad. Sci.*, 2012, **109**, 15589–15593.
25 C. Costentin, S. Drouet, M. Robert and J.-M. Saveant, *J. Am. Chem. Soc.*, 2012, **134**, 11235–11242.
26 C. Costentin, S. Drouet, M. Robert and J. M. Saveant, *Science*, 2012, **338**, 90–94.
27 C. Costentin and J.-M. Saveant, *ChemElectroChem*, 2014, **1**, 1226–1236.
28 A. M. Appel and M. L. Helm, *ACS Catal.*, 2014, **4**, 630–633.
29 K. Izutsu, *Acid-Base Dissociation Constants in Dipolar Aprotic Solvents*, Blackwell Scientific: Oxford, U.K, 1990.
30 S. Daniele, P. Ugo, G. A. Mazzocchin and G. Bontempelli, *Anal. Chim. Acta*, 1985, **173**, 141–148.
31 S. E. Smith, J. Y. Yang, D. L. DuBois and R. M. Bullock, *Angew. Chem., Int. Ed.*, 2012, **51**, 3152–3155.
32 J. A. S. Roberts and R. M. Bullock, *Inorg. Chem.*, 2013, **52**, 3823–3835.
33 R. Mecke, *Discuss. Faraday Soc.*, 1950, 161–177.
34 C. M. French and I. G. Roe, *Trans. Faraday Soc.*, 1953, **49**, 314–323.
35 J. F. Coetzee and G. R. Padmanab, *J. Am. Chem. Soc.*, 1965, **87**, 5005–5010.
36 J.-M. Savéant and E. Vianello, in *Advances in Polarography*, ed. I. S. Longmuir, Pergamon Press, Cambridge, U.K, 1959, pp. 367–374.
37 J.-M. Saveant, *Elements of Molecular and Biomolecular Electrochemistry: an Electrochemical Approach to Electron Transfer Chemistry*, John Wiley & Sons, Hoboken, NJ, 2006.
38 Otherwise, TON and TOF will depend on factors such as the volume of the cell (for a given catalyst concentration, the larger the cell, the less efficient the catalyst!), failing to provide an intrinsic chemical characterization of the catalyst.
39 These equations are valid for all transient non-destructive techniques and also for steady-state techniques such as rotating-disk electrode voltammetry. In the latter case, forced-convection imposes a steady-state transport regime. Steady-state conditions are imposed in two respects, diffusion takes place under steady-state conditions, because of electrode rotation, on the one hand and because mutual compensation between catalytic reaction and diffusional transport, on the other hand. It is the second of these aspects that counts in the case of fast catalytic reactions, as it transpires from the independence of the whole current-potential curves from the rotation rate deriving from the application of the same eqn (1)–(3) as in the case of cyclic voltammetry.
40 I. Bhugun and J.-M. Saveant, *J. Electroanal. Chem.*, 1996, **408**, 5–14.
41 J.-M. Savéant and K.-B. Su, *J. Electroanal. Chem.*, 1984, **171**, 341–349.
42 F. Quentel and F. Gloaguen, *Electrochim. Acta*, 2013, **110**, 641–645.
43 C. Costentin, H. Dridi and J.-M. Saveant, submitted.
44 I. Bhugun, D. Lexa and J.-M. Saveant, *J. Am. Chem. Soc.*, 1996, **118**, 3982–3983.
45 J. T. Muckerman and E. Fujita, *Chem. Commun.*, 2011, **47**, 12456–12458.
46 B. H. Solis and S. Hammes-Schiffer, *Inorg. Chem.*, 2011, **50**, 11252–11262.
47 J. L. Dempsey, J. R. Winkler and H. B. Gray, *J. Am. Chem. Soc.*, 2010, **132**, 16774–16776.
48 M. L. Helm, M. P. Stewart, R. M. Bullock, M. R. DuBois and D. L. DuBois, *Science*, 2011, **333**, 863–866.
49 U. J. Kilgore, J. A. S. Roberts, D. H. Pool, A. M. Appel, M. P. Stewart, M. R. DuBois, W. G. Dougherty, W. S. Kassel, R. M. Bullock and D. L. DuBois, *J. Am. Chem. Soc.*, 2011, **133**, 5861–5872.
50 C. C. L. McCrory, C. Uyeda and J. C. Peters, *J. Am. Chem. Soc.*, 2012, **134**, 3164–3170.